Last time | Continued / finished working on the gluon-exchange cross-section. Considered a color-singlet $q\bar{q}$ pair scattering on another color-singlet $q\bar{q}$ pair:

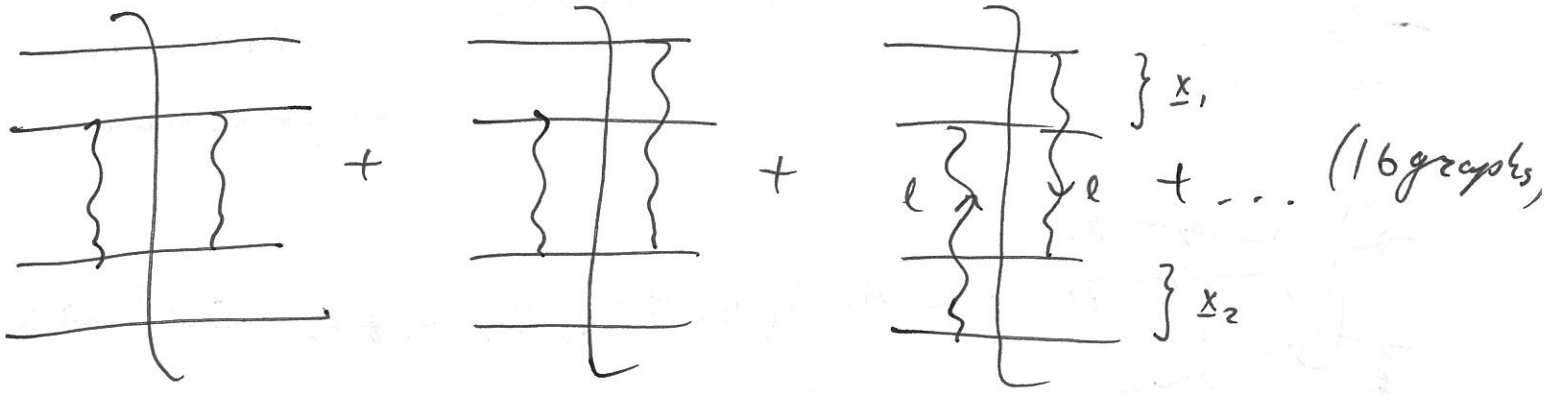

$$\sigma^{\text{onium+onium}} = \frac{2\alpha_s^2 C_F}{N_c}\int \frac{d^2\ell_\perp}{(\ell_\perp^2)^2}\left[2-e^{i\underline{\ell}\cdot\underline{x}_1}-e^{-i\underline{\ell}\cdot\underline{x}_1}\right]\cdot\left[2-e^{i\underline{\ell}\cdot\underline{x}_2}-e^{-i\underline{\ell}\cdot\underline{x}_2}\right].$$

One can integrate this over ℓ while averaging over directions of $\underline{x}_1$ and $\underline{x}_2$ (home work), obtaining

$$\left\langle \sigma^{\text{onium+onium}} \right\rangle = \frac{4\pi\alpha_s^2 C_F}{N_c}\, x_\ell^2\left(\ln\frac{x_7}{x_\ell}+1\right)$$

with $x_{7\ell} = \begin{matrix}\max\\ \min\end{matrix}\{|\underline{x}_1|, |\underline{x}_2|\}$.

Unitarity and Cross Sections (cont'd)

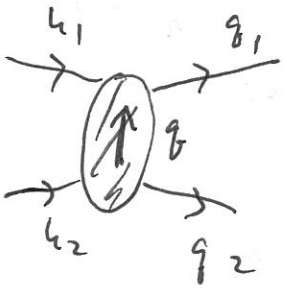

$= i A(k_1, k_2 \to q_1, q_2)$ — elastic $2 \to 2$ scattering amplitude

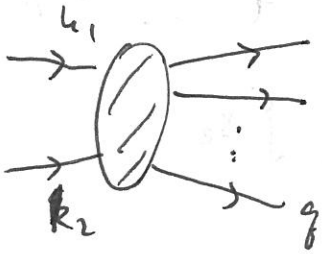

$= i A(k_1, k_2 \to q_1, q_2, \dots, q_n)$ — inelastic scattering amplitude ($n > 2$).

Optical Theorem $\quad \sigma_{tot} = 2\, \mathrm{Im}\, A(k_1, k_2 \to k_1, k_2)$

σ_{tot}: total x-section

$A(k_1, k_2 \to k_1, k_2)$: forward scattering amplitude

On the other hand,

$$\sigma_{tot} = \sigma_{el} + \sigma_{inel} = \int \frac{d^2 q_\perp}{(2\pi)^2} |A(k_1, k_2 \to q_1, q_2)|^2 + \text{inelastic terms}$$

$q = q_1 - k_1 = k_2 - q_2$

go to coordinate space: $\quad A(s,t)$ becomes this, $t = -q_\perp^2$

$$A(k_1, k_2 \to q_1, q_2) = \int d^2 b\, e^{-i \underline{q} \cdot \underline{b}} A(s, \underline{b})$$

$$2\,\mathrm{Im}\,A(k_1,k_2\to k_1,k_2)=\int\frac{d^2q}{(2\pi)^2}\,|A(k_1,k_2\to q_1,q_2|^2+\text{inelastic terms}$$

$$2\,\mathrm{Im}\int d^2b\;A(s,\underline{b})=\int\frac{d^2q}{(2\pi)^2}\int d^2b_1\,d^2b_2\;e^{-i\underline{q}\cdot(\underline{b}_1-\underline{b}_2)}\cdot$$

$$\cdot\,A(s,\underline{b}_1)\,A^*(s,\underline{b}_2)\;+\text{inelastic terms}$$

$$2\,\mathrm{Im}\int d^2b\;A(s,\underline{b})=\int d^2b\;|A(s,\underline{b})|^2+\text{inelastic terms.}$$

Unitarity and Cross Sections

For example, the tree-level diagrams in Fig. B.1 yield

$$\mathrm{Im}_s\, A\left(s', t; \text{Fig. B1a}\right) = \pi\lambda^2\delta\left(m^2 - s'\right), \tag{B.16a}$$

$$\mathrm{Im}_u\, A\left(u', t; \text{Fig. B1b}\right) = \pi\lambda^2\delta\left(m^2 - u'\right). \tag{B.16b}$$

Substituting each of these imaginary parts into the right-hand side of Eq. (B.15) yields the appropriate amplitude after straightforward integration over the delta functions.

Note that a dispersion relation in the form Eq. (B.15) cannot be used in QCD since we know that QCD amplitudes grow in proportion to the energy s at large s (see e.g. Eq. (3.17)), making the integrals in Eq. (B.15) divergent. Therefore, we have to alter Eq. (B.15) by subtracting, for example, the amplitude $A(s = 0, t)$ obtained by putting $s = 0$ in Eq. (B.15). Doing this, we obtain the *subtracted dispersion relation*

$$A(s,t) = A(s=0,t) + \frac{1}{\pi}\left\{ s\int_{s_{min}}^{+\infty} ds' \frac{\mathrm{Im}_s\, A\left(s', t\right)}{s'(s'-s)} + [u - u(s=0)]\int_{u_{min}}^{+\infty} du' \frac{\mathrm{Im}_u\, A\left(u', t\right)}{[u'-u(s=0)](u'-u)} \right\}. \tag{B.17}$$

Finally, subtracting $s\partial_s A(s = 0, t)$ from Eq. (B.17) (with $A(s, t)$ again given by Eq. (B.15)) we obtain the *double-subtracted dispersion relation*

$$A(s,t) = A(s=0,t) + s\partial_s A(s=0,t) + \frac{1}{\pi}\left\{ s^2\int_{s_{min}}^{+\infty} ds' \frac{\mathrm{Im}_s\, A\left(s', t\right)}{s'^2(s'-s)} + [u - u(s=0)]^2\int_{u_{min}}^{+\infty} du' \frac{\mathrm{Im}_u\, A\left(u', t\right)}{[u'-u(s=0)]^2(u'-u)} \right\}. \tag{B.18}$$

This is exactly the dispersion relation used in Eq. (3.43). Note that in perturbative QCD $A(s = 0, t) = 0$.

B.2 Unitarity and the Froissart–Martin bound

The unitarity constraint (B.3) can be written in terms of scattering amplitudes as (see e.g. Peskin and Schroeder (1995))

$$M(k_1, k_2 \to k_1, k_2) - M^*(k_1, k_2 \to k_1, k_2) = i\sum_{n=2}^{\infty}\int\prod_{i=1}^{n}\frac{d^3q_i}{(2\pi)^3 2E_{q_i}} |M(k_1, k_2 \to q_1, \ldots, q_n)|^2 (2\pi)^4\delta^4\left(k_1 + k_2 - \sum_{j=1}^{n} q_j\right), \tag{B.19}$$

where $M(k_1, k_2 \to q_1, \ldots, q_n)$ is the $2 \to n$ scattering amplitude for the scattering of two particles with momenta k_1, k_2 into n particles with momenta $q_1, \ldots, q_n$, and $M(k_1, k_2 \to k_1, k_2)$ is the forward scattering amplitude; E_{q_i} is the energy of a particle with momentum q_i.

Let us consider the case of high energy scattering, where k_1^+ and k_2^- are very large and so are $q_1^+ \approx k_1^+$ and $q_2^- \approx k_2^-$. Separating the *elastic* $2 \to 2$ contribution from the *inelastic* contributions ($2 \to 3$, $2 \to 4$, etc.) on the right-hand side of Eq. (B.19), and integrating over the delta-function in that contribution, yields

$$2\,\mathrm{Im}\, A(k_1, k_2 \to k_1, k_2) = \int\frac{d^2q_\perp}{(2\pi)^2}|A(k_1, k_2 \to q_1, q_2)|^2 + \text{inelastic terms}, \tag{B.20}$$

where q is the momentum transfer four-vector, defined by

$$q = q_1 - k_1 = k_2 - q_2, \tag{B.21}$$

and we also define a new rescaled scattering amplitude

$$A(k_1, k_2 \to q_1, q_2) \equiv \frac{M(k_1, k_2 \to q_1, q_2)}{2\sqrt{2E_{k_1} 2E_{k_2} 2E_{q_1} 2E_{q_2}}} \approx \frac{M(k_1, k_2 \to q_1, q_2)}{2k_1^+ k_2^-}. \tag{B.22}$$

Since both the incoming and outgoing particles are on mass shell the momentum transfer q has only two free components, which we choose to be transverse and over which we integrated in Eq. (B.20).

The optical theorem then states that the total scattering cross section is given by (again, see e.g. Peskin and Schroeder (1995))

$$\sigma_{tot} = 2 \,\mathrm{Im}\, A(k_1, k_2 \to k_1, k_2) \tag{B.23}$$

so that Eq. (B.20) simply implies that

$$\sigma_{tot} = \sigma_{el} + \sigma_{inel}, \tag{B.24}$$

where σ_{el} is the elastic $2 \to 2$ cross section and σ_{inel} is the total inelastic cross section.

As we have seen above, in general the elastic amplitude $A(k_1, k_2 \to q_1, q_2)$ can be written as a function of the Mandelstam variables s and t. However, for our purposes it is convenient to go to impact parameter ($\vec{b}_\perp$) space, using

$$A(k_1, k_2 \to q_1, q_2) = \int d^2b e^{-i\vec{q}_\perp \cdot \vec{b}_\perp} A(s, \vec{b}_\perp), \tag{B.25}$$

which, when applied in Eq. (B.20) yields

$$2 \,\mathrm{Im}\, A(s, \vec{b}_\perp) = |A(s, \vec{b}_\perp)|^2 + \text{inelastic terms}. \tag{B.26}$$

In arriving at Eq. (B.26) we have used the fact that the forward amplitude corresponds to the case of zero momentum transfer, $t = 0$, or, equivalently, $q_\perp = 0$, such that

$$A(k_1, k_2 \to k_1, k_2) = \int d^2b A(s, \vec{b}_\perp). \tag{B.27}$$

Note that the total cross section in impact parameter space is

$$\sigma_{tot} = 2 \int d^2b \,\mathrm{Im}\, A(s, \vec{b}_\perp). \tag{B.28}$$

We also see immediately from Eq. (B.26) that the elastic cross section is given by

$$\sigma_{el} = \int d^2b \, |A(s, \vec{b}_\perp)|^2. \tag{B.29}$$

Relating the inelastic terms in Eq. (B.26) to the corresponding cross section yields

$$2\mathrm{Im}A(s, \vec{b}_\perp) = |A(s, \vec{b}_\perp)|^2 + \frac{d\sigma_{inel}}{d^2b}. \tag{B.30}$$

The simple nonnegativity condition

$$\frac{d\sigma_{inel}}{d^2b} \geq 0 \tag{B.31}$$

used in Eq. (B.30) yields

$$\mathrm{Im}\, A(s, \vec{b}_\perp) \leq 2. \tag{B.32}$$

$2\,\mathrm{Im}\,A = (\mathrm{Re}\,A)^2 + (\mathrm{Im}\,A)^2 + \frac{d\sigma_{inel}}{d^2b}$

$2\,\mathrm{Im}\,A - (\mathrm{Im}\,A)^2 - (\mathrm{Re}\,A)^2 \geq 0$ $\quad |1 - \mathrm{Im}\,A| \leq 1$

$1 - (1 - \mathrm{Im}\,A)^2 \geq (\mathrm{Re}\,A)^2 \geq 0 \Rightarrow$ $\quad 0 \leq \mathrm{Im}\,A \leq 2$

This is an important condition, which follows from unitarity. When used in Eq. (B.28) it yields an upper bound for the total cross section:

$$\sigma_{tot} = 2\int d^2b\ \mathrm{Im}A(s,\vec{b}_\perp) \le 4\int d^2b = 4\pi R^2, \tag{B.33}$$

where R is the radius of the region in $b_\perp$-space where the interactions are sufficiently strong (the radius of the "black disk").

Parametrizing the forward scattering amplitude by (as follows from $S = I + iT$)

$$A(s,\vec{b}_\perp) = i\Big[1 - S(s,\vec{b}_\perp)\Big], \tag{B.34}$$

with $S(s,\vec{b}_\perp)$ the forward matrix element of the S-matrix, we see that the constraint (B.32) and the nonnegativity of the total cross section σ_{tot} together lead to $|\mathrm{Re}S(s,\vec{b}_\perp)| \le 1$.

Using Eq. (B.34) in Eqs. (B.28), (B.29), and (B.30) yields

$$\sigma_{tot} = 2\int d^2b\ \Big[1 - \mathrm{Re}S(s,\vec{b}_\perp)\Big], \tag{B.35a}$$

$$\sigma_{el} = \int d^2b\ \Big|1 - S(s,\vec{b}_\perp)\Big|^2, \tag{B.35b}$$

$$\sigma_{inel} = \int d^2b\ \Big[1 - |S(s,\vec{b}_\perp)|^2\Big]. \tag{B.35c}$$

In high energy scattering the bound on the total cross section is even stronger than Eq. (B.33). At very high energies inelastic processes dominate, so that $\sigma_{inel} \ge \sigma_{el}$, which leads to

$$\mathrm{Re}S(s,\vec{b}_\perp) \ge 0. \tag{B.36}$$

With the help of Eq. (B.34) we obtain

$$\mathrm{Im}A(s,\vec{b}_\perp) \le 1, \tag{B.37}$$

which is a stronger constraint than (B.32). Equation (B.37) leads to

$$\sigma_{tot} = 2\int d^2b\ \mathrm{Im}A(s,\vec{b}_\perp) \le 2\pi R^2. \tag{B.38}$$

This is the bound used in the text in Eq. (3.112). (For a derivation of this result in nonrelativistic quantum mechanics see Landau and Lifshitz (1958), vol. 3, Chapter 131.) Using the estimate (3.115) for the typical interaction range, i.e.,

$$R = b^* \sim \frac{\Delta}{2m_\pi}\ln s, \tag{B.39}$$

in Eq. (B.38) yields the Froissart–Martin bound (3.116)

$$\sigma_{tot} \le \frac{\pi\Delta^2}{2m_\pi^2}\ln^2 s \tag{B.40}$$

(Froissart 1961, Martin 1969, Lukaszuk and Martin 1967).

where M^0 is the single-gluon exchange amplitude given in Eq. (3.17). Note that Eq. (3.111) is in effect the same as Eq. (3.53), which we employed in deriving the BFKL evolution equation.

Equation (3.107) represents the so-called "bootstrap" idea, which states that the evolution of the reggeized gluon is given by the evolution of the color-octet t-channel state of two gluons. It is referred to as the *bootstrap equation*. It has been conjectured that the bootstrap equation (3.107) with its rather simple solution (3.108) holds at any order in α_s. (Indeed both $K^{(8)}_{NF}$ and ω_G receive corrections at higher orders in α_s: the conjecture states that these corrections leave Eqs. (3.107) and (3.108) in exactly the same form as shown above, only modifying $K^{(8)}_{NF}$ and ω_G in them.) So far the conjecture has been verified at the two lowest orders in α_s: the leading order-α_s result is presented here, and the validity of the bootstrap equation at order α_s^2 has been shown by Fadin, Kotsky, and Fiore (1995, 1996).

We see that the bootstrap equation (3.107) with its solution leading to Eq. (3.111) implies that the nonforward BFKL equation for the color-octet state of two gluons should lead to a reggeized gluon with the Regge trajectory $\alpha_G(q_\perp) = 1 + \omega_G(q_\perp)$. This observation completes the proof that in high energy scattering a t-channel gluon should be treated as a reggeized gluon whose spin depends on its transverse momentum.

3.3.6 Problems of BFKL evolution: unitarity and diffusion

The BFKL equation represents an important step towards understanding the high energy asymptotics of QCD. Nonetheless, as for every major scientific advance, the BFKL equation raises some important questions, which we will describe in this section. In particular we will show that as the collision energy increases (i) the leading-logarithmic BFKL equation violates unitarity and (ii) the transverse momenta of the gluons inside the BFKL ladder tend to drift to both the UV and IR, the latter drift eventually leading to a violation of the assumption of the perturbative nature of the interactions.

The Froissart–Martin bound

We begin our presentation of the unitarity bound with a discussion of the black disk limit. Imagine the high energy scattering of a point particle on a "black disk" of radius R. Using the language of nonrelativistic quantum mechanics one can think of the black disk as an infinite potential well occupying a spherical region of space. It can then be shown that the total cross section for the scattering of the point particle from the disk is limited from above by

$$\sigma_{tot} \leq 2\pi R^2 \tag{3.112}$$

(see Landau and Lifshitz (1958), vol. 3, Chapter 131, and the discussion in Appendix B). The total cross section can be as large as twice the geometric cross sectional area of the disk: this doubling is due to Babinet's principle in optics, which states that the diffractive patterns of complementary screens are identical (see Jackson (1999) or Landau and Lifshitz (1958), vol. 2, Chapter 61). In optics Babinet's principle implies that the amount of light

diffracted by a screen is equal to the amount of light it absorbs. For very high energy scattering it implies that, when the scattering occurs from a black disk, the elastic (σ_{el}) and inelastic (σ_{inel}) cross sections are equal. Since the inelastic cross section is equal to the cross sectional area of the disk πR^2, we have $\sigma_{el} = \sigma_{inel} = \pi R^2$, so that the total cross section is $\sigma_{tot} = \sigma_{inel} + \sigma_{el} = 2\pi R^2$.

Our derivation of the Froissart–Martin bound will incorporate the argument put forward by Heisenberg (1952, 1939) with the proof devised by Froissart (1961) and Martin (1969). Consider hadron–hadron scattering at impact parameter b. Let us assume that b is large enough that the black-disk limit described above has not been reached. Inspired by the above examples of the BFKL equation and the Low–Nussinov pomeron, we may assume that the interaction between the hadrons is accomplished though an exchange of one or several particles, so that the cross section grows as some positive power Δ of the energy: $\sigma \sim s^{\Delta}$. At the same time the strength of the interaction should fall off as we increase b: the steepest physically possible fall off is the exponential $e^{-2m_\pi b}$, where m_π is the mass of the lightest QCD bound state, the pion.[7] (As the pion has negative parity, the exchange of a single pion cannot contribute to the total cross section, hence we need to exchange two pions, one in the amplitude and the other in the complex-conjugate amplitude.) We thus have a probability p of interaction that scales with energy and impact parameter as follows:

$$p \sim s^{\Delta} e^{-2m_\pi b}. \tag{3.113}$$

The interaction gets strong when the probability is of order 1. In fact, for p of order 1 the black-disk-limit behavior should begin to set in. Thus the upper limit on the radius of the black disk can be determined by requiring that $p \approx 1$, which, as we can see from Eq. (3.113), occurs at impact parameter b^* defined by

$$s^{\Delta} e^{-2m_\pi b^*} = 1, \tag{3.114}$$

which gives

$$R = b^* \sim \frac{\Delta}{2m_\pi} \ln s. \tag{3.115}$$

Since b^* is the upper bound on the black-disk radius, the total cross section, dominated by the black-disk contribution, is then limited by $2\pi R^2 = 2\pi b^{*2}$, yielding eventually

$$\sigma_{tot} \leq \frac{\pi \Delta^2}{2m_\pi^2} \ln^2 s. \tag{3.116}$$

We conclude that the total cross section in QCD cannot grow faster than the logarithm of energy squared. Equation (3.116) is known at *the Froissart–Martin bound* and was first rigorously proven by Froissart (1961) and Martin (1969) (see also Lukaszuk and Martin (1967)).

[7] As discussed by Nussinov (2008), it is possible that for realistic estimates the pion mass in this exponential should in fact be replaced by the mass of the lightest glueball (a QCD bound state having no valence quarks) since, as we have seen above, gluons dominate in high energy interactions.

As we saw above (see e.g. Eq. (3.87)), the BFKL equation in the diffusion approximation implies that the total cross section grows as a power of the energy,

$$\sigma_{tot}^{BFKL} \sim s^{\alpha_P - 1}, \tag{3.117}$$

which clearly violates the Froissart–Martin bound (3.116). Things do not get much better in the double logarithmic limit of the BFKL equation, which, according to Eq. (3.91), gives

$$\sigma_{tot}^{DLA\ BFKL} \sim \exp\left\{2\sqrt{\bar{\alpha}_s \ln s \ln(l_\perp^2/l'^2_\perp)}\right\}, \tag{3.118}$$

where $l_\perp$ and $l'_\perp$ are the momentum scales at the two ends of the BFKL ladder, with $l_\perp \gg l'_\perp$ in the DLA. The energy growth of the cross section in Eq. (3.118) is exponential in $\sqrt{\ln s}$, and, as such, is much faster than any power of $\ln s$: therefore, DLA BFKL also violates the Froissart–Martin bound. Note that since DLA BFKL is equivalent to DLA DGLAP, the DGLAP evolution also violates unitarity, making this an inherent problem of standard perturbative QCD: no matter how high the larger perturbative scale $l_\perp$ is, at sufficiently high energy s, unitarity will still be violated, as follows from Eq. (3.118). We thus conclude that unitarity violation happens at perturbatively large momentum scales, where perturbative QCD is still applicable. Thus, it is natural to expect that the resolution of this problem should also happen through a QCD perturbative mechanism. We will discuss shortly how a nonlinear evolution equation was proposed by Gribov, Levin, and Ryskin (GLR) to remedy this problem of the BFKL evolution (Gribov, Levin, and Ryskin 1983).

One may indeed argue that in deriving the Froissart–Martin bound above we have used the fact that QCD is a confining theory with bound states such as, which one certainly does not see in the perturbative calculations leading to the BFKL equation. Therefore, since the QCD mass gap m_π is not present in perturbation theory (which has a zero mass gap), one should not expect BFKL evolution to satisfy the Froissart–Martin bound. This argument is indeed correct; however, as we will show below, the BFKL equation can also be written in impact parameter space. As we argue in Appendix B, in impact parameter space the high energy cross sections are given by

$$\sigma_{tot} = 2\int d^2b \left[1 - \mathrm{Re}S(s, \vec{b}_\perp)\right], \tag{3.119a}$$

$$\sigma_{el} = \int d^2b \left|1 - S(s, \vec{b}_\perp)\right|^2, \tag{3.119b}$$

$$\sigma_{inel} = \int d^2b \left[1 - |S(s, \vec{b}_\perp)|^2\right], \tag{3.119c}$$

with $S(s, \vec{b}_\perp)$ the forward matrix element of the scattering S-matrix. Since at high energy $S \to 0$ we see that $d\sigma_{tot}/d^2b_\perp \leq 2$, which is equivalent to the black-disk limit (3.112). The BFKL-dominated total cross section at a fixed impact parameter b grows as a power of the energy s, eventually violating the bound $d\sigma_{tot}/d^2b_\perp \leq 2$ at very high energy. Thus the BFKL equation violates unitarity not only through the fast growth of the black-disk radius but also by the fact that the cross section at each impact parameter becomes larger than the black-disk bound $d\sigma_{tot}/d^2b_\perp \leq 2$. While the former problem cannot be remedied in QCD

4

Dipole approach to high parton density QCD

We are now ready to present more recent developments in high energy QCD. We will consider DIS in the rest frame of a proton or a nucleus. In this frame a virtual photon fluctuates into a quark–antiquark pair, which, in turn, hits the proton or nuclear target. We argue that quark–antiquark dipoles are convenient degrees of freedom for high energy scattering in QCD. We will present a simple model of DIS on a nucleus, due to Glauber, Gribov, and Mueller, in which the $q\bar{q}$ dipole rescatters multiple times on a nuclear target consisting of independent nucleons. We then include quantum corrections to this multiple-rescattering picture: we argue that the initial $q\bar{q}$ dipole may develop a cascade of gluons before hitting the target nucleus. In the large-N_c limit the cascade is described by Mueller's dipole model. When applied to DIS the dipole cascade resummation leads to the Balitsky–Kovchegov (BK) nonlinear evolution equation. We describe approximate analytical and exact numerical solutions of the BK equation and show that it resolves both problems of BFKL evolution: BK evolution is unitary and has no diffusion into the IR. It generates a saturation scale Q_s that grows with energy, justifying the use of perturbative QCD. We conclude the chapter by presenting the Bartels–Kwiecinski–Praszalowicz (BKP) evolution equation for multiple reggeon exchanges, along with the evolution equation for (C-odd) odderon exchange.

4.1 Dipole picture of DIS

Let us begin by considering DIS in the rest frame of the proton or nucleus. While many conclusions in this chapter may also apply to proton DIS, in the strict sense our results would be justified only for DIS on a large nucleus since such a nucleus has a large atomic number parameter A allowing us to make the approximations we will need below. We will therefore only talk about DIS on a nuclear target.

Without any loss of generality we can choose a coordinate axis such that the momentum of the virtual photon is given by

$$q_\mu = \left(q_+, -\frac{Q^2}{q_+}, 0_\perp\right) \tag{4.1}$$

in the $(+, -, \perp)$ light cone notation. The light cone momentum of the virtual photon q_+ is very large (since the (high) photon–nucleus center-of-mass energy is $\hat{s} = mq^+$), so that its

P1: SFK Trim: 247mm × 174mm Top: 13.707mm Gutter: 18.98mm
CUUK1947-04 CUUK1947/Kovchegov 978 0 521 11257 4 March 23, 2012 20:28

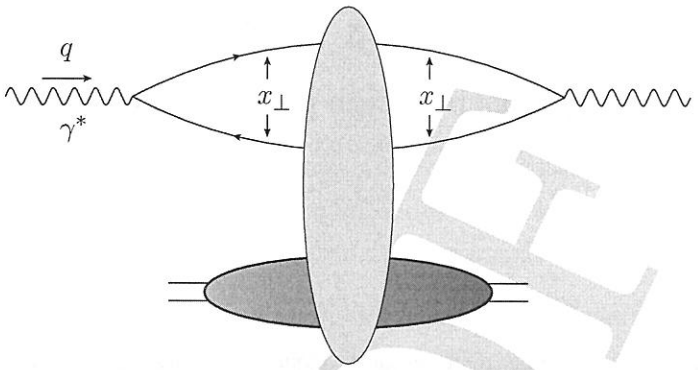

Fig. 4.1. Forward scattering amplitude for DIS on a proton or nuclear target in the rest frame of the target: the virtual photon splits into a $q\bar{q}$ pair which then interacts with the target. The interaction is depicted by the vertical oval. For simplicity the electron that emits the virtual photon is not shown.

coherence length in the longitudinal plus direction (see Sec. 2.3 above),

$$x^+ \approx \frac{2}{|q^-|} = \frac{2q^+}{Q^2}, \tag{4.2}$$

is much larger than the size of the nucleus. If the virtual photon fluctuates into a quark–antiquark pair, the typical lifetime of such a $q\bar{q}$ fluctuation would also be much longer than the nuclear diameter. Therefore, a DIS process in the nuclear rest frame occurs when a virtual photon fluctuates into a $q\bar{q}$ pair (which we will also refer to as a color dipole or simply a dipole); the $q\bar{q}$ pair proceeds to interact with the target (Gribov 1970, Bjorken and Kogut 1973, Frankfurt and Strikman 1988). The forward scattering amplitude for the process is pictured in Fig. 4.1, with the $q\bar{q}$ dipole–nucleus interaction represented by the vertical oval. This is the dipole picture of DIS (Kopeliovich, Lapidus, and Zamolodchikov 1981, Bertsch *et al.* 1981, Mueller 1990, Nikolaev and Zakharov 1991). Note that while the topology of the DIS diagram in Fig. 4.1 is the same as for DIS in the IMF, shown in Fig. 2.2, the time-ordering of the interactions is different in the two figures.

The interaction of a virtual photon with a nucleus can be viewed as a two-stage process: the virtual photon decays into a colorless dipole consisting of a quark and an antiquark and the colorless dipole travels through the nucleus. However, this separation between the time scale for the photon to decay into the $q\bar{q}$ pair and the interaction time is not the only advantage of the dipole picture. Another important simplification comes from the fact that in high energy scattering a colorless dipole, with transverse size $x_\perp$, does not change its size during the interaction and therefore the S-matrix of the interaction is diagonal with respect to the transverse dipole size (Zamolodchikov, Kopeliovich, and Lapidus 1981, Levin and Ryskin 1987, Mueller 1990, Brodsky *et al.* 1994). Indeed, while the colorless dipole is traversing the target, the distance $x_\perp$ between the quark and antiquark can only

vary by an amount

$$\Delta x_\perp \approx R\frac{k_\perp}{E} \tag{4.3}$$

where $E \sim q^0$ denotes the energy of the dipole in the laboratory frame (the target rest frame), R is the longitudinal size of the target, and $k_\perp$ is the relative transverse momentum of the $q\bar{q}$ pair acquired through interaction with the target. In Eq. (4.3) $k_\perp/E$ is the relative transverse velocity of the quark with respect to the antiquark. From Eq. (4.3) we can see already that the change in the dipole size is suppressed by a power of the energy E and is therefore small. To quantify this better let us first remember the definition of Bjorken x, given in (2.2):

$$x = \frac{Q^2}{2P\cdot q} = \frac{Q^2}{mq^+} \approx \frac{Q^2}{2mE}. \tag{4.4}$$

Using Eq. (4.4) in Eq. (4.3) along with the uncertainty principle $Q \approx k_\perp \approx 1/x_\perp$ yields

$$\frac{\Delta x_\perp}{x_\perp} \approx 2mxR = \frac{4R}{l_{coh}} \ll 1, \tag{4.5}$$

where $l_{coh} = 2/(mx)$ is the coherence length of the dipole fluctuation (see Eq. (2.56)). We thus see that at small $x \ll 1/(mR)$, when the dipole interacts with the whole nucleus coherently in the longitudinal direction, the transverse recoil of the quark and the antiquark are negligible compared with the size of the dipole. Therefore the transverse size of the dipole is invariant in high energy interactions, as indicated in Fig. 4.1.

We conclude that in calculating the total DIS cross section, along with other high energy QCD observables, it is convenient to work in transverse coordinate space. We will therefore adopt a mixed representation: we will use longitudinal momentum space along with transverse coordinate space. Light cone perturbation theory (LCPT) is a very useful tool here again. Using LCPT to calculate the total DIS $\gamma^* A$ cross section we can factorize the diagram in Fig. 4.1 into the square of the light cone wave function $\Psi^{\gamma^*\to q\bar{q}}(\vec{x}_\perp, z)$ for the splitting of a virtual photon into a $q\bar{q}$ dipole and the total cross section for the scattering of a dipole on a target nucleus $\sigma_{tot}^{q\bar{q}A}(\vec{x}_\perp, Y)$, so that

$$\sigma_{tot}^{\gamma^* A}(x, Q^2) = \int \frac{d^2x_\perp}{4\pi} \int_0^1 \frac{dz}{z(1-z)} |\Psi^{\gamma^*\to q\bar{q}}(\vec{x}_\perp, z)|^2 \sigma_{tot}^{q\bar{q}A}(\vec{x}_\perp, Y). \tag{4.6}$$

Here $z = k^+/q^+$, with k^+ the light cone momentum of the quark in the $q\bar{q}$ pair. In general the dipole–nucleus cross section will depend on z too; however, in the eikonal and LLA approximations that we mainly consider below, $\sigma_{tot}^{q\bar{q}A}$ is independent of z. The net rapidity interval for the dipole–nucleus scattering is given by $Y = \ln(\hat{s}x_\perp^2) \approx \ln 1/x$ for $x_\perp \sim 1/Q$.

The reader may have other doubts about the factorization (4.6): after all, the LCPT rules presented in Sec. 1.3 require us to subtract the light cone energy of the incoming state in the energy denominator from each intermediate state's energy. Since the light cone energy of the incoming virtual photon is $q^- = -Q^2/q^+$, it seems that each intermediate state that

P1: SFK Trim: 247mm × 174mm Top: 13.707mm Gutter: 18.98mm
CUUK1947-04 CUUK1947/Kovchegov 978 0 521 11257 4 March 23, 2012 20:28

we have absorbed into $\sigma_{tot}^{q\bar{q}A}(\vec{x}_\perp, Y)$ should "know" about the photon's energy. However, in the rest frame of the nucleus, q^- is equal to $-Q^2/q^+ \sim 1/\hat{s}$ and is therefore negligibly small compared with the typical minus components of momenta involved in dipole–nucleus interactions. The same would be true for dipole–nucleus scattering: the incoming dipole state would have a negligibly small light cone energy compared with the energies involved in the interaction. Therefore, in our eikonal approximation (up to corrections of order $1/\hat{s}$), we can interchange the negligible light cone energy q^- for the light cone energy of the dipole without changing the answer, thus justifying the factorization of Eq. (4.6). (Note that in calculating the light cone wave function $\Psi^{\gamma^* \to q\bar{q}}(\vec{x}_\perp, z)$ we cannot neglect the light cone energies of the virtual photon and the $q\bar{q}$ dipole, since they are the only terms entering the energy denominator.) Another important assumption is that the light cone energy of the target is not modified until the interaction with the dipole: one can show that the time scale of target fluctuations is much shorter than the lifetime of the dipole. Hence the target does not affect the virtual photon's wave function, since in constructing the latter the same light cone energy of the target enters into both the energies of the intermediate states and the initial-state energy, thus canceling in the energy denominators.

The factorization of Eq. (4.6) is very convenient: it allows us to separate the simple $\gamma^* \to q\bar{q}$ QED process from the strong interaction dynamics contained in $\sigma_{tot}^{q\bar{q}A}(\vec{x}_\perp, Y)$.

Note that the virtual photon may have either transverse or longitudinal polarization. Requiring that the photon polarization satisfies $\epsilon \cdot q = 0$ and imposing $\epsilon_T^2 = -1$ for transverse polarization and $\epsilon_L^2 = 1$ for the longitudinal polarization, we obtain for q^μ, Eq. (4.1), the following polarizations:

$$\epsilon_T^\lambda = (0, 0, \vec{\epsilon}_\perp^\lambda), \tag{4.7a}$$

$$\epsilon_L = \left(\frac{q^+}{Q}, \frac{Q}{q^+}, \vec{0}_\perp\right), \tag{4.7b}$$

with $\vec{\epsilon}_\perp^\lambda$ as given in Eq. (1.54). The polarization vectors (4.7) form a complete basis in the space of possible polarizations, so that the numerator of the photon propagator in the Landau gauge can be decomposed in terms of them as

$$g_{\mu\nu} - \frac{q_\mu q_\nu}{q^2} = -\sum_{\lambda=\pm} \epsilon_{T\mu}^\lambda \epsilon_{T\nu}^{\lambda *} + \epsilon_{L\mu} \epsilon_{L\nu}^*. \tag{4.8}$$

Using the polarizations (4.7) along with Eqs. (2.13) and (2.16) one can separate the total DIS cross section into transverse (T) and longitudinal (L) components (see Halzen and Martin 1984):

$$\sigma_T^{\gamma^* A} = \frac{4\pi^2 \alpha_{EM}}{q^0} W^{\mu\nu} \frac{1}{2} \sum_{\lambda=\pm} \epsilon_{T\mu}^\lambda \epsilon_{T\nu}^{\lambda *} = \frac{4\pi^2 \alpha_{EM}}{q^0} W_1 \tag{4.9a}$$

$$\sigma_L^{\gamma^* A} = \frac{4\pi^2 \alpha_{EM}}{q^0} W^{\mu\nu} \epsilon_{L\mu} \epsilon_{L\nu}^* = \frac{4\pi^2 \alpha_{EM}}{q^0} \left[-W_1 + \left(1 + \frac{\nu^2}{Q^2}\right) W_2\right], \tag{4.9b}$$

with ν as defined in Eq. (2.5) and α_{EM} the fine structure constant. Employing Eqs. (2.18a) and (2.18b), we can rewrite Eqs. (4.9) in the high energy $\nu \gg Q$ limit as expressions for